International Journal of Innovative
Computing, Information and Control
Volume **17**, Number **1**, February **2021**

 ISSN 1349-4198
pp. 31–47

DETECTION OF FISHBONES IN FISH FLOSS PRODUCTS USING CURVELET TRANSFORM BASED SQUARE-RING BAND-HIGHPASS FILTERING TECHNIQUES

Hong-Dar Lin[1,*], Chang-Yi Lin[1] and Chou-Hsien Lin[2]

[1]Department of Industrial Engineering and Management
Chaoyang University of Technology
No. 168, Jifong East Road, Wufong District, Taichung 41349, Taiwan
*Corresponding author: hdlin@cyut.edu.tw

[2]Department of Civil, Architectural, and Environmental Engineering
The University of Texas at Austin
301, East Dean Keeton Street, Austin, Texas 78712-0273, USA

Received August 2020; revised December 2020

Abstract. *Both fish and fish-related products are common foodstuffs for many cultures around the world. Fish floss is a preserved fish product made from finely chopped or mashed fish, which are boiled in seasonings and then stir-fried until the mass is arid and pulverous. During consumption, fishbones constitute the most frequently ingested extraneous objects. In the making of commercial fish floss, fishbone inspection is currently conducted by experienced inspectors who use their sense of touch and sight to detect bones. This reliance on human inspection leaves considerable room for error, which poses a consumer health risk as fishbones may cause physical harm when ingested. This study seeks to replace the human inspectors in this process by exploiting a frequency filtering method based on computer vision to inspect fishbones in fish floss products. The proposed method applies the curvelet transform with square-ring band-highpass energy filtering to removing the random patterns of background and to deleting the angle direction of background texture. The approximated and partially detailed components regarding fishbones and uniform background are preserved in the low and medium frequency bands; the filtered image is then inversely converted to spatial domain. In the reconstructed image, the background random texture is attenuated and the fishbone areas are enhanced. Experimental outcomes show that the suggested inspection method can effectively identify and locate the visible fishbones, and outperforms the existing methods of fishbone inspection on the bumpy, irregularly textured surfaces of fish floss products.*

Keywords: Processed fish products, Fish floss, Curvelet transform, Fishbone detection, Band filtering, Visual inspection system

1. **Introduction.** Both fish and fish-related products are common foodstuffs for many cultures around the world, providing protein and other macronutrients necessary to maintain good physical condition. The main form of direct consumption of raw fish, cooked fish, processed products (such as preserved fish, canned fish, and fish floss) is fairly extensive. Fish floss is a processed product that is produced from fresh fish through a process of grinding, frying, and adding spices and additives for flavor [1]. It is made from finely chopped or mashed fish boiled in seasonings, then stir-fried until the mass is arid and pulverous. This fish floss is usually eaten with steamed rice, porridge, or slices of white bread. It is a versatile source of protein that can complement many carbohydrate staples.

DOI: 10.24507/ijicic.17.01.31

Figure 1 shows five common types of fish floss products: salmon floss, tuna floss, swordfish floss, milkfish floss, and lizardfish floss, each made from the respective fish species. Different kinds of fish floss have various surface textures and colors. This study uses the swordfish floss as our testing sample product.

FIGURE 1. Common types of fish floss products: (a) salmon floss; (b) tuna floss; (c) swordfish floss; (d) milkfish floss; (e) lizardfish floss

The procedure for processing fish into floss comprises six general steps: collecting and selecting raw materials, separating fish meat, making seasonings, boiling, cooking, and packaging the produced fish floss [2]. Some defects in fish floss can result from incomplete separation and cleaning of fish meat, unsuitable temperature controls of ovens, and inappropriate stir-fry operations during the production. Figure 2 illustrates the specific dimensions of fishbones for four different sizes used in this study: small, medium, large, and extra-large. Larger fishbones are usually removed in the stage of separating fish meat, but some medium- and small-sized fishbones may be left in fish meat. When fish is usually eaten, fishbones are certain of the most regularly gulped extraneous objects. In the making of commercial fish floss, fishbone inspection is conducted by experienced inspectors who use their sense of touch and sight to detect bones. This reliance on human inspection leaves considerable room for error, which poses a consumer health risk as fishbones may cause physical harm when ingested. Figure 3 shows the manual inspection method currently used in commercial fish floss production. Not only is manual inspection tiresome and laborious, it also depends heavily on the inspectors' expertise. Exhaustion and eyestrain, and indeed the subjectivity of the inspectors themselves, often allow fishbones and bone fragments to make their way into the final product. When consumers then eat the fish floss, they become at risk of ingesting the fishbones, which, depending on the size and orientation, can cause severe injuries. Therefore, this study proposes a vision-based defect inspection system for commercial fish floss production. The inspection of fishbone defects is the major concern in this study.

The fried fish floss samples need be spread out evenly on a platform before capturing images by using a vision system. Obstruction describes the portion of each fishbone that is hidden beneath the layer of fish floss, and is not detected by the visual system. Figure

	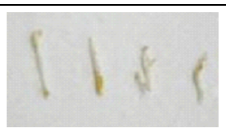			
Size	Small	Medium	Large	Extra Large
Length	10 ~ 15 (mm)	16 ~ 25 (mm)	26 ~ 30 (mm)	> 30 (mm)
Width	1 ~ 1.5 (mm)	1.6 ~ 2.0 (mm)	2.1 ~ 2.6 (mm)	> 2.6 (mm)

FIGURE 2. Dimensions of fishbones for four different sizes

FIGURE 3. Traditional human inspection using hands to remove defects in fish floss products

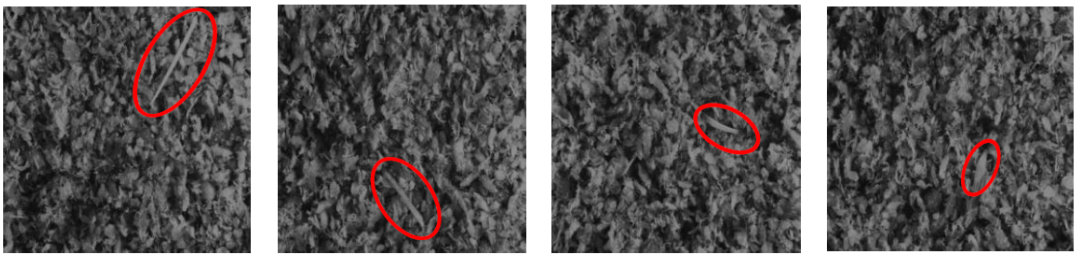

FIGURE 4. Fish floss images with different fishbone obstruction percentages: (a) 0%; (b) 30%; (c) 50%; (d) 70%

4 depicts four fish floss images with different fishbone obstruction percentages: 0%, 30%, 50%, and 70%. The detectable fishbone size in this study to be inspected out is with length greater than 10 mm and width larger than 1 mm. Since the fish floss samples are spread out evenly on a platform in advance, the fishbones tend to migrate towards the surface of the fish floss. The goal of this work is to explore the use of an optical system to detect the near-surface fishbones in fish floss samples. The identification of fishbones in fish floss is difficult because the bumpy surface of the spread fish floss introduces variations to the sample depth, producing properties in the image that can conceal small fishbones. In addition, since the textured fish floss has the appearance of random patterns, those evident textures make the fault identification work with more difficulty when visible fishbones are inlaid on the bumpy exteriors with random textures. We therefore propose a curvelet transform based approach to resolving these problems of automated fishbone inspection in fish floss products.

Curvelet transform is one kind of multi-resolution transform involving multi-layer decomposition and reconstruction. It is an extension of the wavelet transform, exhibiting better directionality and reconstruction [3]. The use of curvelet transform is suggested for enhancement of fishbone images in defect inspections that also include images with natural-looking details. Curvelet transform has superior directional and edge expression capabilities compared with the widely used wavelet transform. Encouraged by these excellent properties, this study proposes the method of breaking down images into its curvelet bands and employing square-ring band-highpass energy filtering on the selected bands to attenuate textured patterns of fish floss and enhance fishbones in the rebuilt image. The proposed approach, based on computer vision, can substitute for human inspectors in the traditional fishbone inspection tasks during fish floss production.

The rest of the article is composed as follows. Firstly, we review the articles on modern techniques of image processing for defect detection in food products. Secondly, we depict

the proposed curvelet transform based approach for inspecting fishbones in fish floss products. Thirdly, we conduct the experiments and evaluate the performance of the proposed techniques with existing methods. Finally, based on the findings of the experiments, we draw conclusions and suggestions for future development.

2. **Literature Review.** Machine vision offers an automatic, non-contact, and cost-effective option to achieve the requirement for precise, rapid and impartial quality inspection in many industrial applications [4-7]. The automated detection methods based on image analysis and pattern recognition techniques have created various applications in the food industry, such as detection of maturity levels of fresh tomatoes [8], ripeness classification of cape gooseberry fruits [9], quality classification of pre-sliced pork meats and turkey hams [10], and meat quality evaluation of different meat products [11]. These food and agricultural applications can all decrease labor-intensive inspection and increase goods quality as well as productivity by reducing both inspection time and human errors [12,13].

Some studies investigate the quality inspection of fish related products. Since fishbones are some of the most regularly ingested extraneous objects during consumption, fishbone detection is the main task in quality inspection of fish products [14]. Han and Shi [15] combined particle swarm clustering and morphological operations in fishbone detection for radiographic images. Thielemann et al. [16] used texture analysis of surface images to forecast fishbone locations in fish fillets. Sivertsen et al. [17] applied a ridge detection method to finding the centerline on cod fillets for quality inspection. Mery et al. [18] proposed an X-ray computer vision method to inspect fishbones in fish fillets of salmon and trout. Rerkratn and Kaewpoonsuk [19] developed a quality assessment system for fish fillets employing K-means clustering and thresholding skills. The fish fillet quality is evaluated based on percent of fish fillet and fishbone region. From the aforementioned literature, almost all of the presented fishbone detection methods were developed for fish fillets [14-19] and through radiographic images [14,15,18]. Those developed systems are expensive for the X-ray related devices. In addition, these researches do not inspect defects with attributes of small fishbones on bumpy exteriors of fish floss products. Accordingly, this study applies curvelet transform filtering approach to defect detection on bumpy surfaces of fish floss and implements a low-cost vision system for fishbone inspection on fish floss products.

As existing filtering techniques for detecting specific patterns along boundaries in object images, there are approaches that use an inverse filter and two Laplacian filters for image restoration and edge enhancement [20], wavelet transform with low-pass filtering for contour fault strengthening [21], and Fourier transform with multi-crisscross filtering for structural texture elimination [22]. The curvelet transform was invented to mitigate the drawbacks of usual two-dimensional (2-D) discrete wavelet transforms. Curvelets constitute a valid model thinking over a multiscale time-frequency local partition as well as utilizing the direction of geometric features. The curvelet transform offers a nearly optimal sparse expression of objects in 2-D cases. Its quickness and simplicity also facilitate the wide implementations of curvelets in many scientific and engineering fields. Boubchir and Fadili [23] statistically examined the components' dependencies of the images covering position, scale and direction in curvelet domain for image restoration applications. Jiang and Zhao [24] developed a curvelet method to reach better denoising results and had the extensive applicability for remote sensing images. Zhang et al. [25] proposed a curvelet transform based method to improve performance of Canny edge operator in tire shearography images.

Some studies proposed mixed methods based on curvelet transform for classifications, such as combining with morphological feature extraction method to characterize non-stochastic surfaces for metrology [26], fusing with Kirsch's templates to extract retinal blood vessels for detection of diabetes at early stages [27], integrating with PCA method to extract features from still images for face recognition [28]. AlZubi et al. [29] applied wavelet, ridgelet, and curvelet transforms, to developing an image separation system for segmenting area of interest in medical images received from various medical sensors.

3. **Proposed Curvelet Transform-Based Approach.** This study presents a curvelet transform (CT) based band-highpass filtering approach to inspect fishbones on surfaces of evenly-spread fish floss products. Six steps are developed to perform the process of fishbone inspection. First, image preprocessing resizes testing images to the specified dimension, 256×256 pixels, to shorten the wait time related to further image processing analysis. Second, forward frequency transform is used to convert the resized spatial domain image to CT domain based on the specified CT parameters, scale and angle. Third, frequency filtering is conducted, applying square-ring band-highpass filtering in CT domain by selecting a suitable decomposition level and a proper square-ring scope; the low-frequency parts exceeding the scope are retained and the remainders are given to zero for reconstructing the image surface. Fourth, the image is reconstructed by executing the inverse curvelet transform on the filtered frequency image. Thus, a fishbone-enhanced image could be rebuilt from the CT domain for contrasting with the initial image. Fifth, interval estimation and object separation are conducted to classify the rebuilt image into two categories (dark fishbones and white background) by applying a statistical interval estimation, in which some features of the identified fishbones are extracted. Sixth, the performance of the suggested inspection method is evaluated and compared to those of existing methods. Figure 5 describes the flow chart of the proposed approach.

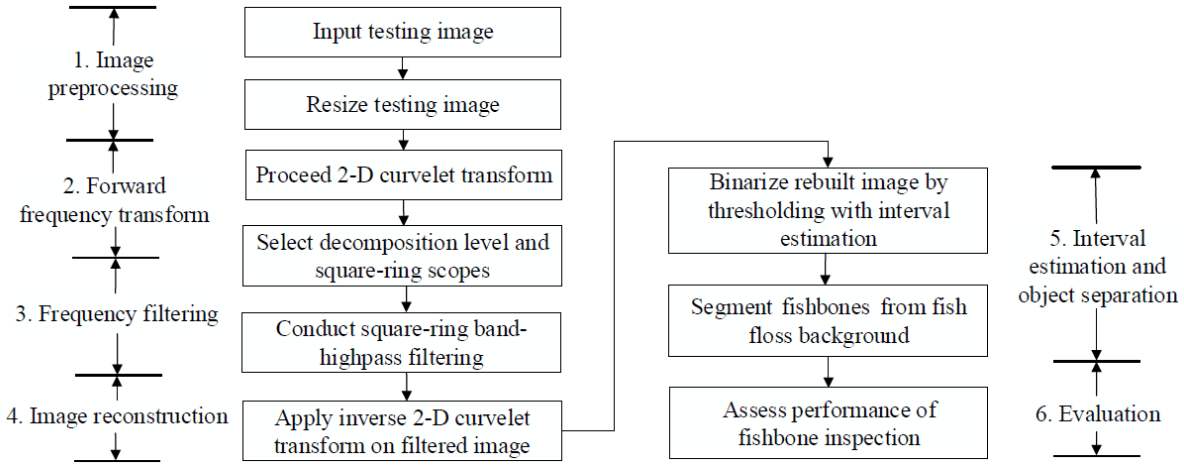

FIGURE 5. Flow chart of the suggested CT based band-highpass filtering approach

3.1. **Curvelet transform.** Curvelet transform was invented by Candès and Donoho in 2000 [30] applying ridgelet analysis to radon transform. The CT is distinctive in its computation as it calculates coefficients at every scale, orientation and position. For discrete image analysis, the feed in image is in the format of a Cartesian array; therefore, the rotation alters to shear and the computation arises in a pseudo-polar coordinate plane [31]. The CT is an expansion of the wavelet transform revealing superior directionality and rebuilding. Candès et al. suggested a revised version of CT, called fast discrete

curvelet transform (FDCT) being quicker, easier and reduced redundant than the original ridgelet transform [32].

The FDCT in this study is executed via a wrapping-based method, taking advantage of its simplicity of execution and shorter processing time. The wrapping-based FDCT is a multiscale pyramid including distinct orientations and positions in frequency domain. It employs merits of fast Fourier transform (FFT) in Fourier spectral domain. In the process of FFT, the image and curvelet with a specified scale and direction are converted into the Fourier domain. After transformation process, we gain a set of curvelet coefficients through reverse FFT to the spectral product. This set includes curvelet coefficients in rising sequence of the scales and directions.

FDCT utilizing frequency wrapping is employed to the transformed image to gain curvelet coefficients through computing image orientation from distinct angles. The stages of FDCT approach based on wrapping applied to this study are summarized as the following [32].

Step 1. A testing image $f(x, y)$ with $N \times N$ size is converted into the frequency domain by forward 2-D FFT,

$$F[u, v] = \frac{1}{N^2} \sum_{x=0}^{N-1} \sum_{y=0}^{N-1} f(x, y) \exp[-j \cdot 2\pi(ux/N + vy/N)]. \tag{1}$$

Step 2. The transformed image $F[u, v]$ is then multiplied by a set of discrete localizing window functions $\tilde{U}_{j,l}$. For every scale j and orientation l, it forms the product $\tilde{U}_{j,l}[u, v]F[u, v]$. The shapes of these windows are defined in accordance with the conditions of the ideal CT.

Step 3. The products on these districts are wrapped around the origin into rectangular shape,

$$\tilde{F}_{j,l}[u, v] = W\left(\tilde{U}_{j,l}F\right)[u, v]. \tag{2}$$

Step 4. Apply the inverse 2-D FFT to each wrapped coefficient,

$$f'(x, y) = \sum_{u=0}^{N-1} \sum_{v=0}^{N-1} \tilde{F}_{j,l}[u, v] \exp[j \cdot 2\pi(ux/N + vy/N)]. \tag{3}$$

Step 5. Gather the discrete curvelet coefficients $c^D(j, l, k)$ from the inversed FFT image $f'(x, y)$, where j, l, k represent the scale, orientation, and position parameters,

$$c^D(j, l, k) = \sum_{0 \le x, y < n} f'(x, y) \cdot \phi^D_{j,l,k}[x, y]. \tag{4}$$

Each $c^D(j, l, k)$ represents a discrete curvelet waveform.

These coefficients are then filtered out, adopting a highpass filtering regulation which chooses the scope of square-ring bands. The filtered coefficients are obtained after the highpass filtering procedure. The rebuilt image is obtained by applying inverse FDCT on the filtered coefficients.

3.2. **Approximated coefficients and detailed coefficients in curvelet domain.**

Curvelet transform can span the whole frequency space at different scales and directions taking less coefficients for a specified exactness of reconstruction. After decomposition of a discrete image applying curvelet transform based on wrapping method, low, medium and high frequency components of the image at each scale are gained. The low-frequency coefficients, called approximated components, are abundant in information regarding background details of an image as well as the medium- and high-frequency coefficients, called detailed components, convey details mostly regarding the edges existing in

an image. Figure 6 displays a testing image with size 256×256 is performed 1 to 4 decomposition levels of curvelet transformations. The figures show the curvelet coefficients at various scales in 1 to 4 decomposition levels. The central part is the approximated components with low-frequency coefficients; meanwhile, the multiple square-ring bands (marked in black) are the detailed components with high-frequency coefficients. The higher the decomposition levels of CT are conducted, the larger the band-widths of the square-ring bands are obtained. For each band, it is further partitioned into some districts with distinct polar angles. Figure 7 illustrates the 5-level curvelet domain, a schematic diagram indicating the names of various square-ring bands, and a conceptual diagram showing the energy partitions at different bands. The numbers of energy partitions at different square-ring bands in the 5-level curvelet domain are 16, 32, 32, 64. The locations of energy partitions at different bands could describe the relationship between the detailed components and filtering angles.

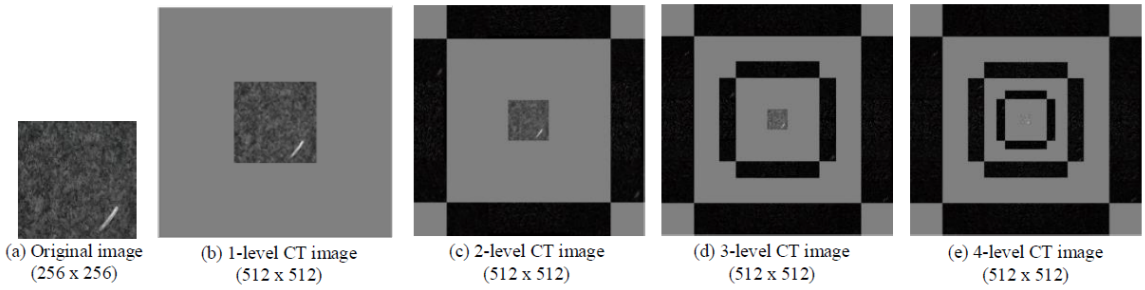

FIGURE 6. A testing image with size 256×256 is performed 1 to 4 decomposition levels of curvelet transformations.

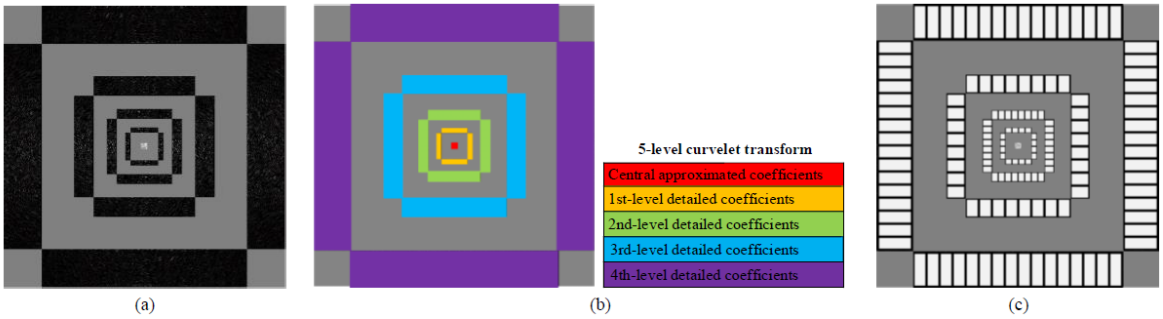

FIGURE 7. A testing image is performed 5-level curvelet transformation: (a) 5-level CT image; (b) a schematic diagram for various square-ring bands; (c) a conceptual diagram for energy partitions at different bands.

Since the wrapping-based FDCT employs the FFT merits in Fourier spectral domain, the wrapped products in Equation (2) with the components of the Fourier transform are complex quantities,

$$\tilde{F}_{j,l}[u,v] = R_{j,l}(u,v) + I_{j,l}(u,v) \tag{5}$$

where

$$R_{j,l}(u,v) = \frac{1}{N^2} \sum_{u=0}^{N-1} \sum_{v=0}^{N-1} \tilde{F}_{j,l}[u,v] \cdot \cos[2\pi(ux/N + vy/N)],$$

and

$$I_{j,l}(u,v) = \frac{1}{N^2} \sum_{u=0}^{N-1} \sum_{v=0}^{N-1} \tilde{F}_{j,l}[u,v] \cdot \sin[2\pi(ux/N + vy/N)].$$

The power spectrum is explained as the square of Fourier spectrum,

$$P_F(u,v) = \left|\tilde{F}_{j,l}[u,v]\right|^2 = R^2_{j,l}(u,v) + I^2_{j,l}(u,v). \tag{6}$$

Figure 8 shows the corresponding 3-D energy histograms for a normal image and a defective image (Figure 6(a)). Both of the 3-D energy histograms show the central part of the approximated components and the square-ring bands of the detailed components gather much more energy in curvelet domain. To realize the energy distributions in various levels of the detailed components, we analyze individual energy plots in each square-ring bands. Figure 9 indicates the energy histograms of detailed components for each selected square-ring band in a 5-level CT image. The red areas in the curvelet domain images are the selected square-ring bands of detailed components to analyze the energy plots.

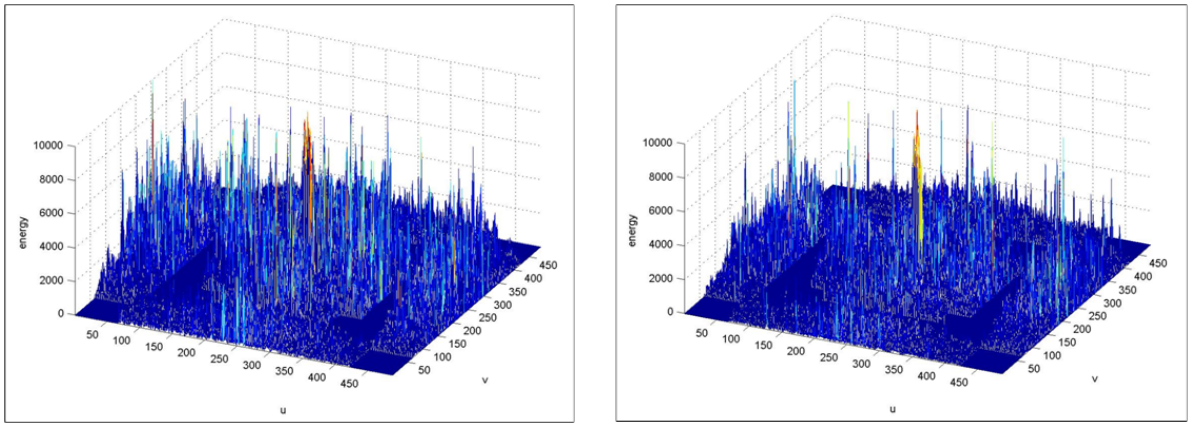

(a) 3-D energy histogram of a normal image (b) 3-D energy histogram of a defective image

FIGURE 8. The 3-D energy histograms for (a) a normal image, and (b) a defective image

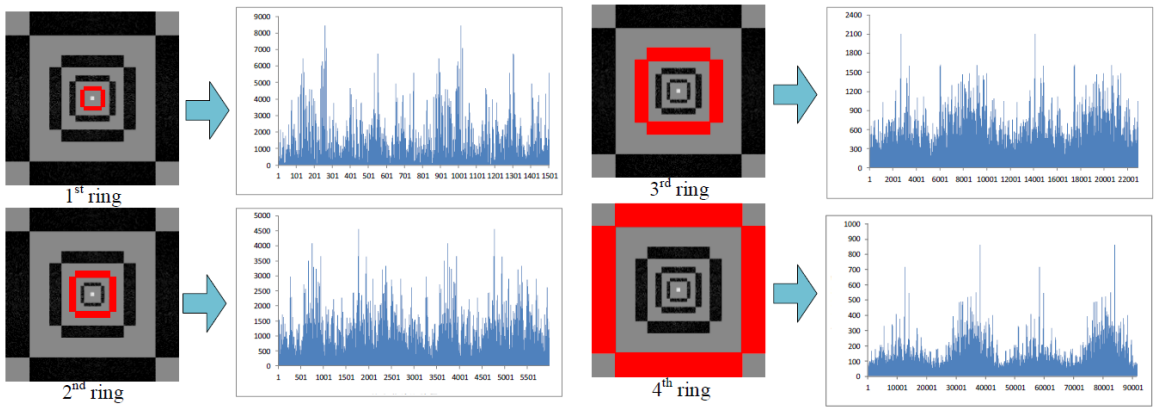

FIGURE 9. (color online) The energy histograms of detailed components for each selected square-ring band in a 5-level CT image

3.3. **Curvelet square-ring band-highpass filtering operation.** Curvelet is an edge based multiscale expression of the image, with the edge details corresponding to bigger curvelet coefficients. The edge details can be expressed with the bigger coefficients in high frequency bands. The highest band normally corresponds to the frequency response of isolated points and noises; thence the frequency response of the edge characteristics

should be found at the sub-highest frequency bands. To further investigate the filtering effect on the images with random texture, the fish floss images are conducted the curvelet square-ring band-highpass filterings with various scopes of detailed components retained. Different retaining scopes of the curvelet square-ring band-pass filterings significantly influence the detection results.

To select the retaining scope of the curvelet square-ring bands, we define $P_{F\_D}^{n-1}(u,v)$ as the power spectrum of the detailed components in an n-level CT image. The minimax algorithm is utilized to minimize the maximum energy values of the detailed components for each level in curvelet domain. A threshold value T_R^L is defined as,

$$T_R^L = \text{Min}\left\{\text{Max}\left[P_{F\_D}^{n-1}(u,v)\right]\right\}. \tag{7}$$

The purpose of curvelet square-ring band-highpass energy filtering operation is to attenuate the background random texture and enhance the fishbone areas. Contrasted to ordinary band filtering, the suggested square-ring band-highpass energy filtering utilizes the minimax value of power spectrums in each level of detailed components as the threshold to reassign the small and medium frequency elements inside the chosen scope of detailed components in CT domain. The square-ring band-highpass filtering operation is to increase the variability between fish floss background and fishbone faults. The main aim is to remove the random background textures with larger variations in intensity, and retain the fishbones with smaller variations in intensity. We use the notion of decision theory to compute the minimax value and substitute all of the frequency components less than the threshold value by zero. The procedure can be expressed as,

$$F'(u,v) = \begin{cases} 0, & P_{F\_D}^{n-1}(u,v) < T_R^L \\ F(u,v), & \text{otherwise} \end{cases}, \tag{8}$$

where $F'(u,v)$ is a filtered CT frequency image.

After the square-ring band-highpass filtering process, the frequency components with larger power spectrums are left in CT domain. Figure 10 indicates the before and after images conducted by square-ring band-highpass filtering in curvelet and spatial domains. After conducting the band-highpass filtering in the chosen bands and inversely converting the filtered image to spatial domain, the random textures on background are significantly attenuated and become more smooth.

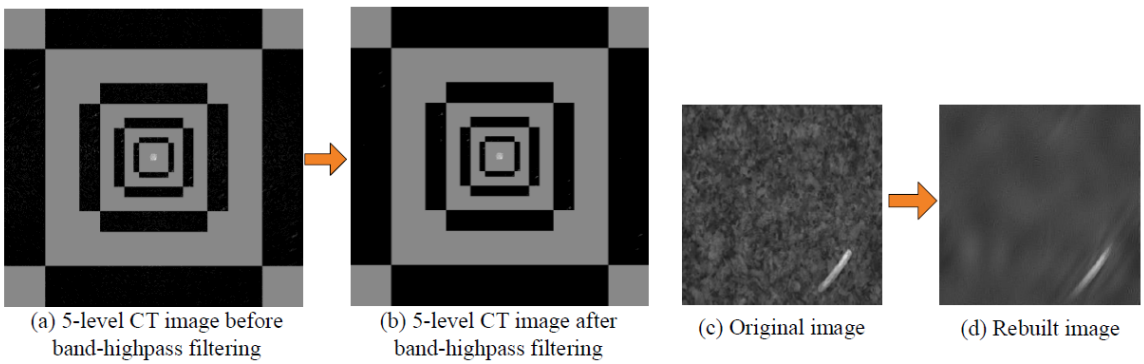

FIGURE 10. Before and after images conducted by square-ring band-highpass filtering in curvelet and spatial domains, respectively

3.4. **Rebuilt filtered image and fishbone separation.** After a proper band scope is determined, the energy filtering process can correctly recognize the low and medium frequency zones of random textures and these frequency components are set to zero in curvelet domain. Next, we take inverse CT on the filtered frequency image to convert

back to time domain for fishbone separation. In this work, we plan to remove many random textures in the rebuilt image by selecting a suitable scope in the detailed components for the zero-value substitute. Because random textures may represent medium power spectrum, rebuilding the detailed components with emphasis region from those of the ordinary textures will erase almost all random textures in an initial image, and preserve exclusively local fishbones in a rebuilt image. The random textures will cause an approximately consistent intensity, while the local fishbones will generate distinct gray levels in the rebuilt image.

The filtered rebuilt image has roughly consistent gray levels for pixels classified to homologous background zones, but it also produces notably distinct gray levels for pixels classified to nonhomologous fishbone districts. The intensity changes in homologous districts could be very little, while the intensity changes in nonhomologous regions could be big contrast to the whole rebuilt image. Thence, this study can determine a threshold for distinguishing fishbones from fish floss area in the reconstructed image. The reconstructed image will be roughly a consistent gray level image if a fish floss product without bones is tested. The upper limit T_U for intensity changes in the rebuilt image is expressed by $T_U = \mu + N\sigma$, where μ and σ are the average and standard deviation of the intensities of the rebuilt image $f'(x, y)$, and N is a controlled parameter decided by experiments. The binary fishbone image $B(x, y)$ for fishbone segmentation is

$$B(x,y) = \begin{cases} 255, & \text{if } f'(x,y) \le (\mu + N\sigma) \\ 0, & \text{otherwise} \end{cases} . \tag{9}$$

If a pixel with the intensity is less than the upper limit T_U, the pixel is categorized as a homologous element. On the contrary, it is categorized as a fishbone element. When the fishbone sizes to be detected are usually very little contrasted to the whole appearance image, the μ and σ can be counted straight from the reconstructed image of an initial image to tolerate the illumination variations in the examination circumstance.

4. **Implementation and Analyses.** This study presents an automatic optical inspection approach for quality assessment of fish floss. To intensify the clearness of object surfaces and fishbones on fish floss products in the phase of image capture, this study utilizes the subsequent devices in the implemented inspection environment: a lighting frame with two incandescent light bulbs, a black and white charge-coupled device camera with 500 M, a lens with 1 to 10 amplifications of changeable focal lengths 13-130 mm, and an electronically controlled table. The vision system adopts an LED ring light attached around the CCD lens and the capture area is 130.2×97.6 mm^2 for each shot. Figure 11 illustrates the schematic diagram of device layout, the hardware setup of the vision system, and dimensions of testing samples spread out evenly on a platform. Assessments are performed on 150 real swordfish floss samples (50 images without fishbones and 100 images with fishbones) to appraise the representation of the proposed method. Every image has a size of 256×256 pixels with a gray level of 8 bits. The fishbone identification arithmetic is edited in MATLAB language and executed on the R2010b version on a computer (INTEL P4-2.8 GHz 512 MB RAM).

To mathematically examine the representation of the recommended technique, we differ the outcomes of our appraisals from those offered by practical examiners (ground truth). The expression guides, $(1 - \alpha)$ and $(1 - \beta)$, are used to express proper inspection assessments; the larger the two guides, the more precise the inspection outcomes. False alarms (α, mistaking fish floss districts as fishbones) are determined by dividing the regions of fish floss districts mistaken as fishbones by the regions of actual fish floss districts. Missed alarms (β, failing to detect actual fishbones) are calculated by dividing the regions of

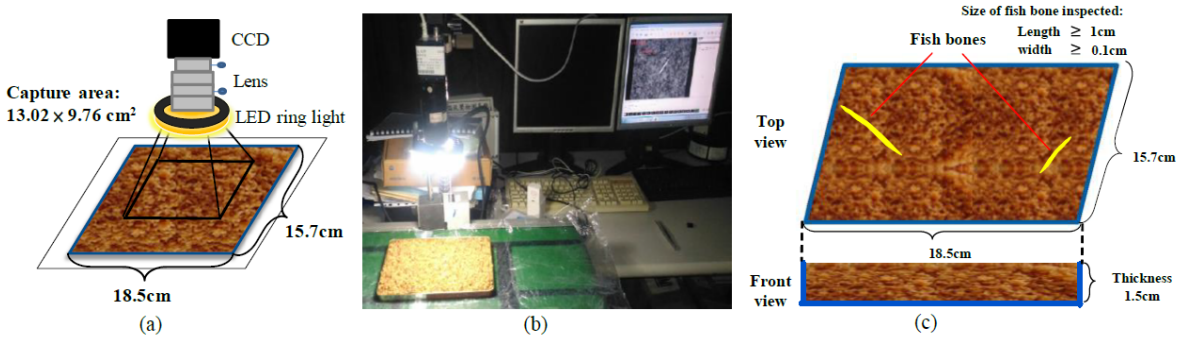

FIGURE 11. Configuration of capturing swordfish floss images: (a) schematic diagram of device layout; (b) hardware setup of the vision system; (c) dimensions of testing samples spread out evenly on a platform

undetected actual fishbones by the regions of all actual fishbones. For both types of error, the lower the guide values, the better the detection outcomes.

4.1. **Parameter settings of the proposed method.** Choice of the key parameter, decomposition level, in the curvelet square-ring band-highpass filtering operation will significantly influence the performance of the proposed method in detecting fishbones. To appraise the influence of altering diverse decomposition levels on rebuilt results, tests display the manifestation guides of inspection outcomes by changing decomposition levels from the range 4 to 7 levels. Figure 12 shows two testing images and the corresponding resulting outcomes by using the suggested method with four decomposition levels. Table 1 presents the fishbone detection results for the four decomposition levels in three performance indices. The figures demonstrate that, at a lower decomposition level (e.g., 4), the proposed method cannot adequately separate fishbones from the fish floss surfaces and misses some alerts. However, at higher decomposition levels (e.g., 6 and 7), the method produces the diverse effect on the fishbones, which causes many false warnings. Decomposition level 5, therefore, is more appropriate to underline fishbones in the curvelet band-highpass filtering domain. Our trials on a variety of testing images have verified that decomposition level 5 is ordinarily appropriate for this particular application.

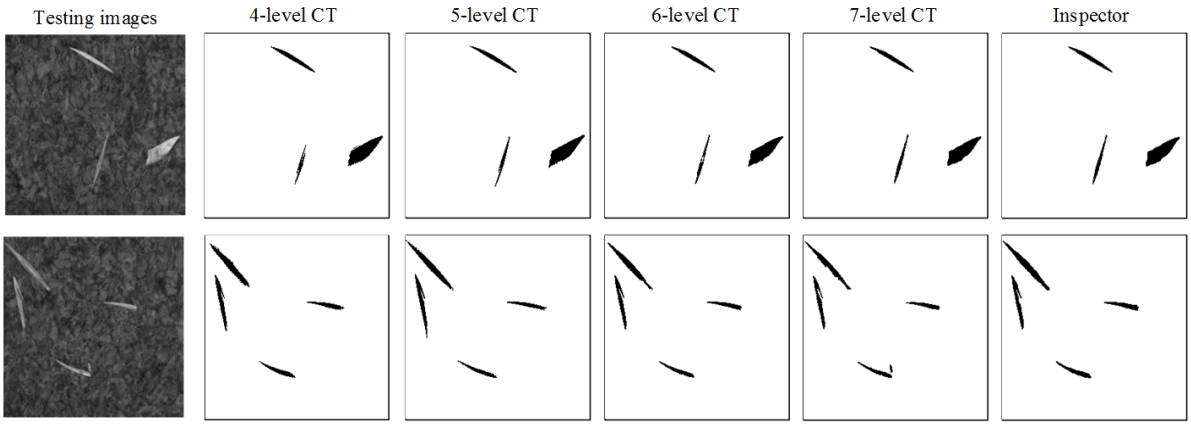

FIGURE 12. Two testing images and resulting outcomes by the proposed CT-based approach with various decomposition levels

TABLE 1. Performance indices of four different decomposition levels in curvelet domain

Decomposition levels	4-level	5-level	6-level	7-level
Fishbone inspection rate $1-\beta$ (%)	81.74	86.30	83.58	82.48
False alarm rate α (%)	0.366	0.149	0.247	0.186
Correct classification rate CCR (%)	99.72	99.77	99.85	99.81

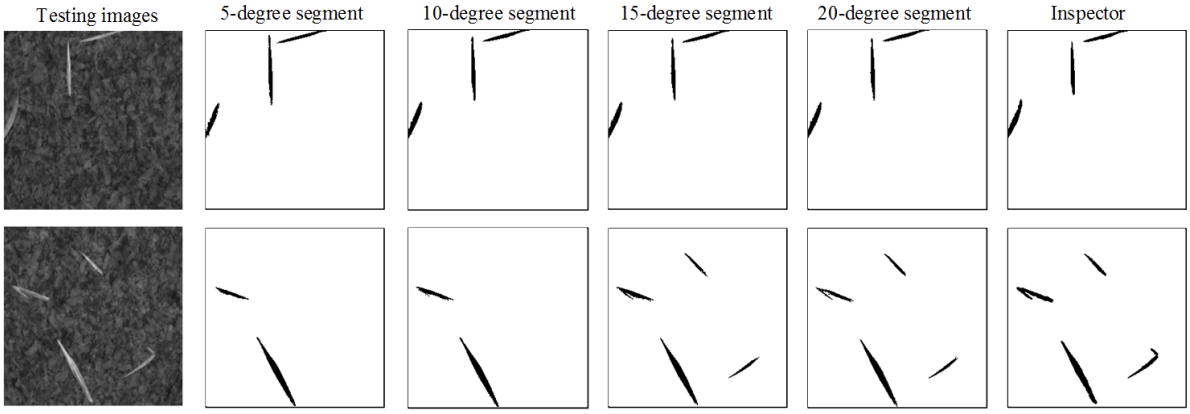

FIGURE 13. Two testing images and resulting outcomes by the proposed CT-based approach with various degree segments

TABLE 2. Performance indices of four different degree segments in curvelet domain

Degree segments	5-degree	10-degree	15-degree	20-degree
Fishbone inspection rate $1-\beta$ (%)	77.94	80.54	86.30	87.03
False alarm rate α (%)	0.108	0.130	0.149	0.206
Correct classification rate CCR (%)	99.47	99.54	99.77	99.57

In the process of fishbone-enhanced filtering in curvelet domain, a suitable degree segment selection is instrumental in accurately differentiating fishbones from fish floss districts. Smaller degree segments will allow the fishbone features to be decomposed more finely and the resulting images will be more detailed. To assess the influence of changing various degree segments in the curvelet filtering operations, tests illustrate the manifestation guides of inspection outcomes by degree segments from the range 5 to 20 degrees. Figure 13 shows two testing images and the corresponding resulting outcomes by using the suggested method and Table 2 presents the fishbone detection results for the four degree segments in three performance indices. The resulting outcomes and the indices indicate that smaller degree segments (e.g., 5 degrees $\sim$ 10 degrees) make baggy controls and may cause some missed alarms, while a bigger degree segment (e.g., 20 degrees) makes a strict control and may lead to some false alarms. The number of degree segment 15 is more appropriate to stress fishbones in the separations of defects from normal fish flosses. The trials on a variety of testing images have confirmed that the 15-degree segment is ordinarily appropriate for this fishbone inspection application.

4.2. **Performance assessment of distinct fishbone detection techniques.** Three existing schemes usually applied to anomaly detection are contrasted to the recommended approach to differentiate effects of fishbone inspection. To indicate the fault inspection outcomes of a testing image, Figure 14 demonstrates fractional outcomes of inspecting fishbones by the Otsu method, the watershed method [33], the discrete wavelet transform

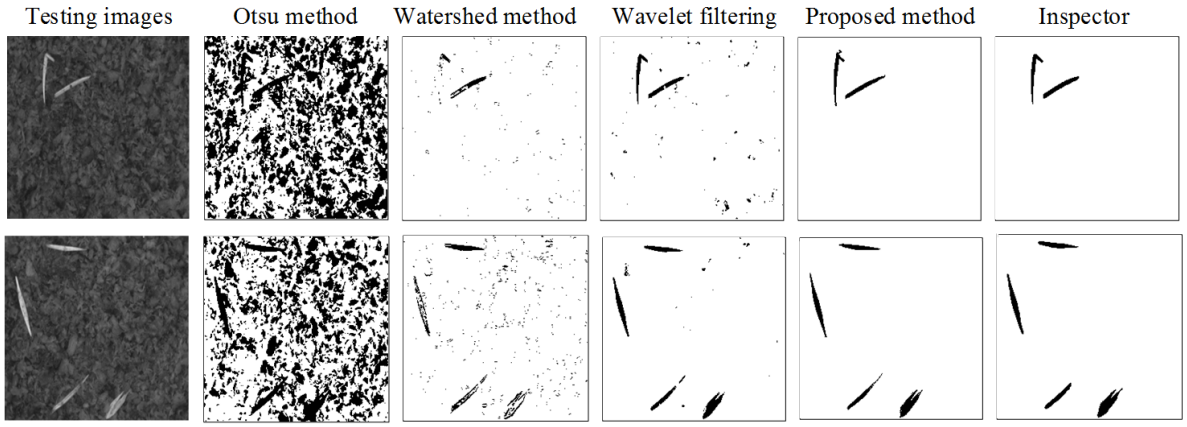

FIGURE 14. Detection outcomes of two testing images for fishbone inspection by Otsu method, watershed method, wavelet filtering method, recommended method, and manual inspection

TABLE 3. Summary table of differentiating effects by four fishbone detection methods

Detection schemes	Otsu method	Watershed method	DWT low-pass filtering method	Suggested method
Fishbone inspection rate $1-\beta$ (%)	99.69	77.71	80.06	86.30
False alarm rate α (%)	89.69	8.08	3.18	0.15
Correct classification rate CCR (%)	58.48	91.80	98.28	99.77
Processing time (sec.)	0.12	0.18	0.77	1.41

(DWT) based low-pass filtering method [34], the recommended method, and the ground truth provided by inspectors, separately. The Otsu method and watershed method produce many erroneous judgments in false alarms and the DWT filtering method causes many of erroneous judgments in missing alarms on appearance fault inspection. The suggested method inspects most of the fishbones and produces less erroneous judgments. Therefore, the suggested technique surpasses the Otsu method, watershed method and DWT low-pass filtering method in the fishbone detection of fish floss products with uneven surfaces.

Table 3 indicates the differentiating effects of fishbone detection consequences in the performed trials. Two spatial domain methods and two frequency domain techniques are evaluated contrary to the consequences by practical examiners. The average fishbone inspection rates $(1-\beta)$ of total trial samples by the three ways are, 99.69% by Otsu method, 77.71% by watershed method, 80.06% by DWT filtering method, and 86.30% by suggested method. However, the three existing techniques have notably larger false alarm rates (α), 89.69% by Otsu method, 8.08% by watershed method, and 3.18% by DWT filtering method. Contrarily, the suggested scheme has quite smaller false alarm rate 0.15%. The suggested method has a larger correct classification rate (CCR), 99.77%, than do the other skills utilized to fishbone detection of fish floss images. More concretely, the suggested approach has a larger fishbone inspection rate as well as has a smaller false alarm rate utilized to fish floss images having high uneven surfaces.

The average computation time for treating an image with 256×256 pixels is as follows: 0.12 seconds by Otsu method, 0.18 seconds by watershed method, 0.77 seconds by DWT filtering method, and 1.41 seconds by recommended method. The mean processing time of the suggested scheme is nearly two times larger than that of the DWT filtering method

yet it can be improved for actual fulfillment of an automatic optical detection system through parallel processing and hardware enhancement. Although the proposed method has a longer processing time, it well balances the trade-off between the fishbone inspection rate (86.30%) and false alarm rate (0.15%), and reaches a correct classification rate of 99.77%, outperforming the traditional defect detection techniques in fishbone inspection of fish floss products.

4.3. **Dynamic visual inspection system.** Since commercial fish floss products are mass produced, this visual inspection system allows the vision solution to handle highly variable inspection times while still being able to meet high production rates. This study extends the developed static inspection system for finding surface fishbones to one that is more dynamic, integrating the hardware and software connections between the inspection system and conveyor related equipment. After the system integrations have been achieved in the dynamic inspection system, the design of experiments and response surface methodology approaches [35] are applied to finding the significant factors that influence the system performance and performing the sequential procedures to reach the optimums of the factors. Figure 15 shows the schematic diagram of device layout and fish floss products are evenly-spread on a conveyor in a dynamic visual inspection system. Table 4 lists a summary inspection performance table for the dynamic visual inspection system under various conveyor speed levels. It indicates that speed level-3 balances the trade-off between the fishbone inspection rate and the inspection time and reaches a correct classification rate of 99.75%, outperforming the other speed levels in fishbone detection of fish floss products. To reduce variations of testing sample depths on an inspection platform, a horizontal vibration device is needed to make fish floss spread out evenly before capturing images. A fishbone absorption device is equipped at the end of the vision system for separating and collecting the detected fishbones. Figure 16 demonstrates a conceptual diagram of gently moving fish floss with a horizontal vibration conveyor and a defect absorption device in the dynamic visual inspection system.

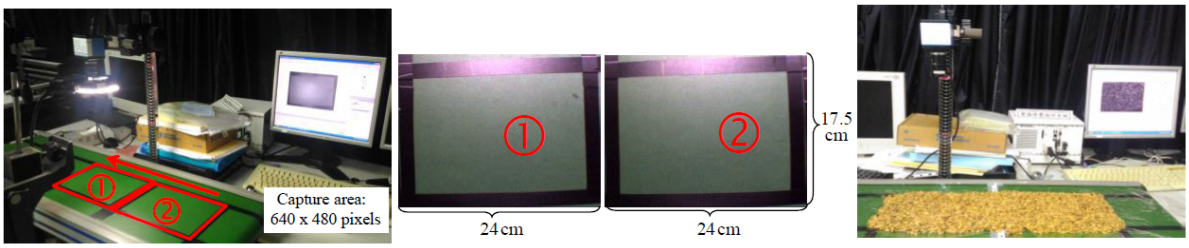

FIGURE 15. Schematic diagrams of device layout and fish floss products are evenly-spread on a conveyor in a dynamic visual inspection system.

TABLE 4. Summary inspection performance table for the dynamic visual inspection system under various conveyor speed levels

Speed levels	Level-1	Level-2	Level-3	Level-4
Real speed (cm/sec.)	7.2	10.4	15.5	20.3
Capture time interval (sec.)	4.06	2.82	1.88	1.45
Fishbone inspection rate $1-\beta$ (%)	90.40	90.26	90.15	84.54
False alarm rate α (%)	0.18	0.17	0.16	0.23
Correct classification rate CCR (%)	99.71	99.74	99.75	99.24

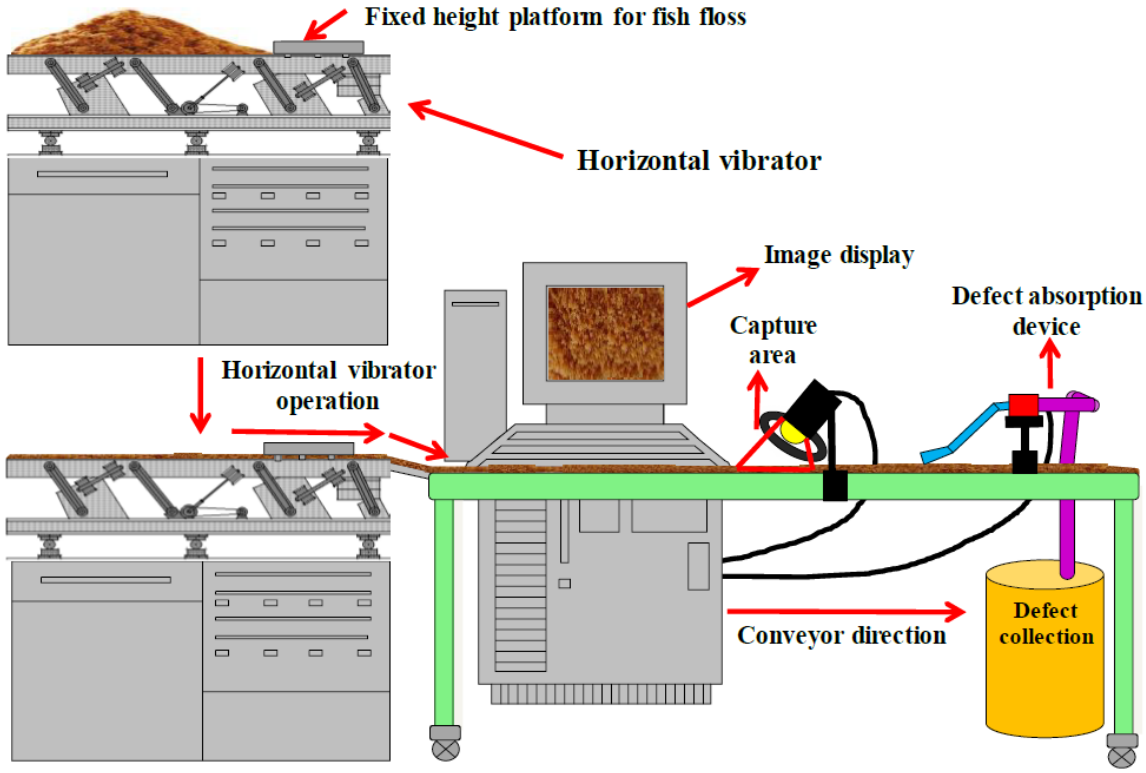

FIGURE 16. A conceptual diagram of gently moving fish floss with a horizontal vibration conveyor and a defect absorption device in the dynamic visual inspection system

5. **Conclusions.** This study proposes a wrapping-based CT approach for fishbone inspection on the bumpy surfaces with random texture of fish floss products. The CT works on images in a comparable pattern as the human visual system, and breaks down images into frequency coefficients at every scale, orientation, and position. The proposed method conducts the square-ring band-highpass energy filtering in frequency domain to remove the random patterns of background and delete the angle direction of background texture. In addition to the effective detection of fishbones along curved edges, the proposed method can also identify fishbones with various shapes in different fish floss textures by changing the decomposition level and degree segment in curvelet domain. Compared to results from the referenced studies, the proposed curvelet-based filtering method entirely surpasses the typical watershed method and the wavelet-based filtering approaches in clarity and detection effectiveness.

Compared to traditional methods, the proposed method may be limited in performance by the additional parameters required, and the processing time may be longer. These parameter settings for the CT filtering model can be prearranged from a training stage in a supervised system. The processing time can be significantly decreased to meet the requests of on-line automatic inspection by implementing the proposed approach in a parallel computing environment or a single integrated circuit. Future research may extend the suggested method to develop a global CT based enhancement approach for detecting surface defects in structural textures and explore the curvelet transform to become an effective solution to texture analysis problems.

Acknowledgment. Authors truthfully appreciate the Ministry of Science and Technology, Taiwan, for the financial assistance through the Grant MOST 108-2221-E-324-006.

REFERENCES

[1] T. Rihayat, Suryani, Zaimahwati et al., Effect of determination temperature on nutrition and organoleptic tuna fish floss, *IOP Conference Series: Materials Science and Engineering*, vol.506, 2019.

[2] I. Wijayanti, T. Surti, A. D. Anggo and E. Susanto, Effect different packaging on proximate and lysine content of milkfish floss during storage, *Aquatic Procedia*, vol.7, pp.118-124, 2016.

[3] J. Ma and G. Plonka, The curvelet transform – A review of recent applications, *IEEE Signal Processing Magazine*, vol.27, no.2, pp.118-133, 2010.

[4] M. S. Alfatni, A. R. M. Shariff, M. Z. Abdullah, O. M. Ben Saeed and O. M. Ceesay, Recent methods and techniques of external grading systems for agricultural crops quality inspection – Review, *International Journal of Food Engineering*, vol.7, no.3, article 10, 2011.

[5] P. B. Pathare, U. L. Opara and F. A. Al-Said, Colour measurement and analysis in fresh and processed foods: A review, *Food Bioprocess Technology*, vol.6, pp.36-60, 2013.

[6] H. D. Lin and K. S. Hsieh, Detection of surface variations on curved mirrors of vehicles using slight deviation control techniques, *International Journal of Innovative Computing, Information and Control*, vol.14, no.4, pp.1407-1421, 2018.

[7] H. D. Lin and H. L. Chen, Detection of surface flaws on textured LED lenses using wavelet packet transform based partial least squares techniques, *International Journal of Innovative Computing, Information and Control*, vol.15, no.3, pp.905-921, 2019.

[8] P. Wan, A. Toudeshki, H. Tan and R. Ehsani, A methodology for fresh tomato maturity detection using computer vision, *Computers and Electronics in Agriculture*, vol.146, pp.43-50, 2018.

[9] M. De-la-Torre, O. Zatarain, H. Avila-George, M. Muñoz, J. Oblitas, R. Lozada, J. Mejía and W. Castro, Multivariate analysis and machine learning for ripeness classification of cape gooseberry fruits, *Processes*, vol.7, no.12, 2019.

[10] A. Iqbal, N. A Valous, F. Mendoza, D.-W. Sun and P. Allen, Classification of pre-sliced pork and Turkey ham qualities based on image color and textural features and their relationships with consumer responses, *Meat Science*, vol.84, pp.455-465, 2010.

[11] G. Elmasry, D. F. Barbin, D.-W. Sun and P. Allen, Meat quality evaluation by hyperspectral imaging technique: An overview, *Critical Reviews in Food Science and Nutrition*, vol.52, no.8, pp.689-711, 2012.

[12] A. Kamilaris and F. X. Prenafeta-Boldu, Deep learning in agriculture: A survey, *Computers and Electronics in Agriculture*, vol.147, pp.70-90, 2018.

[13] K. K. Patel, A. Kar, S. N. Jha and M. A. Khan, Machine vision system: A tool for quality inspection of food and agricultural products, *Journal of Food Science Technology*, vol.49, no.2, pp.123-141, 2012.

[14] K. Andersen, X-ray techniques for quality assessment, in *Quality of Fish from Catch to Consumer: Labelling, Modelling and Traceability*, J. B. Luten, J. Oehlenschlaeger and G. Olafsdottir (eds.), Wageningen Academic Publishers, 2003.

[15] Y. Han and P. Shi, An efficient approach for fish bone detection based on image preprocessing and particle swarm clustering, *Communications in Computer and Information Science*, vol.2, pp.940-948, 2007.

[16] J. T. Thielemann, T. Kirkhus, T. Kavli, H. Schumann-Olsen, O. Haugland and H. Westavik, System for estimation of pin bone positions in pre-rigor salmon, *International Conference on Advanced Concepts for Intelligent Vision Systems (ACIVS2007), Lecture Notes in Computer Science*, vol.4678, pp.888-896, 2007.

[17] A. H. Sivertsen, C. K. Chu, L. C. Wang, F. Godtliebsen, K. Heia and H. Nilsen, Ridge detection with application to automatic fish fillet inspection, *Journal of Food Engineering*, vol.90, pp.317-324, 2009.

[18] D. Mery, I. Lillo, H. Loebel, V. Riffo, A. Soto, A. Cipriano and J. M. Aguilera, Automated fish bone detection using X-ray imaging, *Journal of Food Engineering*, vol.105, pp.485-492, 2011.

[19] A. Rerkratn and A. Kaewpoonsuk, System development for quality evaluation of fish fillet using image processing, *Proc. of the 2014 International Conference on Computer, Communications and Information Technology*, pp.196-199, 2014.

[20] T. Hiraoka, Generation of edge-enhancing labyrinth images using inverse filter and two improved Laplacian filters, *ICIC Express Letters*, vol.14, no.2, pp.121-127, 2020.

[21] H. D. Lin and Y. K. Lin, Automated inspection of contour faults for convex mirrors using wavelet descriptors and EWMA control scheme, *International Journal of Innovative Computing, Information and Control*, vol.16, no.4, pp.1237-1255, 2020.

[22] H. D. Lin and H. H. Tsai, Automated quality inspection of surface defects on touch panels, *Journal of the Chinese Institute of Industrial Engineers*, vol.29, no.5, pp.291-302, 2012.
[23] L. Boubchir and J. M. Fadili, Multivariate statistical modeling of images with the curvelet transform, *IEEE Xplore*, pp.747-750, 2005.
[24] T. Jiang and X. Zhao, Research and application of image denoising method based on curvelet transform, *The International Archives of the Photogrammetry*, vol.62, pp.363-368, 1999.
[25] Y. Zhang, T. Li and Q. Li, Defect detection for tire laser shearography image using curvelet transform based edge detector, *Optics & Laser Technology*, vol.47, pp.64-71, 2013.
[26] L. Li, X. Zhang, H. Zhang, X. He and M. Xu, Feature extraction of non-stochastic surfaces using curvelets, *Precision Engineering*, vol.39, pp.212-219, 2015.
[27] M. Kalaivani, M. S. Jeyalakshmi and V. Aparna, Extraction of retinal blood vessels using curvelet transform and Kirsch's templates, *International Journal of Emerging Technology and Advanced Engineering*, vol.2, pp.360-363, 2012.
[28] T. Mandal and Q. M. J. Wu, Face recognition using curvelet based PCA, *2008 the 19th International Conference on Pattern Recognition*, pp.1-4, 2008.
[29] S. AlZubi, N. Islam and M. Abbod, Multiresolution analysis using wavelet, ridgelet, and curvelet transforms for medical image segmentation, *International Journal of Biomedical Imaging*, DOI: 10.1155/2011/136034, pp.1-18, 2011.
[30] E. J. Candès and D. L. Donoho, Curvelets: A surprisingly effective non-adaptive representation for objects with edges, in *Curve and Surface Fitting: Saint-Malo Proceedings*, A. Cohen, J.-L. Merrien and L. L. Schumaker (eds.), Nashville, TN, Vanderbilt Univ. Press, 2000.
[31] E. J. Candès and D. L. Donoho, New tight frames of curvelets and optimal representations of objects with C^2 singularities, *Communications on Pure and Applied Mathematics*, vol.57, no.2, pp.219-266, 2004.
[32] E. J. Candès, L. Demanet, D. Donoho and L. Ying, Fast discrete curvelet transforms, *Multiscale Modeling & Simulation*, vol.5, no.3, pp.861-899, 2006.
[33] M. Couprie and G. Bertrand, Topological grayscale watershed transformation, *SPIE Vision Geometry VI Proceedings*, vol.3168, pp.136-146, 1997.
[34] Y. P. Chiu and H. D. Lin, Creation of image models for inspecting visual flaws on capacitive touch screens, *Journal of Applied Engineering Science*, vol.16, no.3, pp.333-342, 2018.
[35] D. C. Montgomery, *Design and Analysis of Experiments*, 8th Edition, John Wiley & Sons, New Jersey, USA, 2014.